Remanent magnetization states and interactions in square arrays of 100-nm cobalt dots measured using transmission electron microscopy

T. J. Bromwich,[a] A. Kohn, and A. K. Petford-Long
Department of Materials, University of Oxford, Parks Road, Oxford OX1 3PH, United Kingdom

T. Kasama
Frontier Research System, The Institute of Physical and Chemical Research, Hatoyama, Saitama 350-0305, Japan and the Department of Materials Science and Metallurgy, University of Cambridge, Pembroke Street, Cambridge CB2 3QZ, United Kingdom

R. E. Dunin-Borkowski
Department of Materials Science and Metallurgy, University of Cambridge, Pembroke Street, Cambridge CB2 3QZ, United Kingdom

S. B. Newcomb
Sonsam Limited, Glebe Laboratories, Newport, Co., Tipperary, Ireland

C. A. Ross
Department of Materials Science and Engineering, Massachusetts Institute of Technology, Cambridge, Massachussetts 02139

(Received 14 April 2005; accepted 7 July 2005; published online 13 September 2005)

Large area square arrays of circular cobalt dots, nominally 100 nm in diameter and 20 nm in thickness, were patterned using interference lithography. Magnetic remanent states were measured using off-axis electron holography in the transmission electron microscope (TEM). The results show that the dots are mostly single domain, although vortex states and multidomain configurations are occasionally observed. Significant magnetic interactions between adjacent dots result in variations in their magnetization direction away from the direction of the applied field. The suitability of such dots for data storage applications is discussed. Quantitative magnetic phase measurements were also obtained by applying the transport of intensity equation to images acquired using the Fresnel mode of Lorentz microscopy in the TEM. The consistency between the electron holography and transport of intensity equation (TIE) results is assessed. © *2005 American Institute of Physics*.
[DOI: 10.1063/1.2011780]

I. INTRODUCTION

Magnetic nanodot arrays have been proposed for use in future generations of magnetic recording media.[1,2] The development of interference lithography now allows arrays of nominally identical nanodots to be patterned over an area of several cm^2.[3] It is important to study the magnetic structures of such dots, as well as the magnetic interactions between them, in order to determine their suitability for magnetic information storage applications. Arrays of 200-nm-period cylindrical and conical thin-film Ni and Co dots with a range of heights and diameters have been produced by Ross *et al.*,[4] who used magnetic force microscopy (MFM) and magnetometry to observe transitions from "flower" to "vortex" magnetic states as the dots increased in size. A flower state occurs in a small dot when the magnetization is primarily parallel to a single direction, with small radial deviations at its upper and lower surfaces. A vortex state can be supported in a larger dot, in which the magnetization is perpendicular to the plane of the dot along its axis and tilted into the sample plane in a flux closure configuration around its perimeter. Experimentally, vortex states are observed to occur for base diameters greater than three times the exchange length of the material (7 nm for cobalt) for aspect ratios of 1.5–3 (the aspect ratio R is defined as h/b, where h is the height of the dot and b is the diameter).[4] In addition to this change from a flower to a vortex state, the authors also reported a change in the anisotropy direction at a critical value of the aspect ratio $R_c=0.65$. For dots with $R>R_c$, the out-of-plane direction is an easy axis of magnetization, with the in-plane direction being a hard axis. For flat dots with $R<R_c$, the out-of-plane direction is a hard axis of magnetization. Since the dots described all had circular cross sections, zero in-plane coercivity would be expected. However, in-plane coercivities of between 90 and 220 Oe were measured for Co, and attributed to pinning of the magnetization by edge irregularities, grain boundaries, or other microstructural features as it rotates in plane. Micromagnetic simulations have also been used to predict a transition from an in-plane to an out-of-plane easy axis as a function of dot aspect ratio and spacing.[5] A variation in magnetization reversal field between individual dots was reported by the authors, and it was suggested that this variation arose from interdot interactions, in which the demagnetizing fields of neighboring dots affected the reversal field of the dot in question. Such interactions have been studied by Porrati and Huth,[6] who used micromagnetic simulations to show that significant interactions are expected between nanoscale iron cylinders. They re-

[a]Electronic mail: thomas.bromwich@trinity.ox.ac.uk

ported intercylinder interactions that lower the magnetostatic energy of the system and influence the stability of magnetic configurations. For example, the vortex states that they considered are not stable in cylinders in arrays, while isolated cylinders do show such states.

Magnetization reversal can be investigated using MFM, Lorentz transmission electron microscopy (LTEM), or by applying bulk magnetometry measurements, such as the use of superconducting quantum interference device (SQUID) or alternating-gradient magnetometry to an ensemble of dots. In the case of MFM and LTEM, an external magnetic field is applied to the sample in a chosen direction, and magnetization reversal states are then imaged *in situ*. Little work has been conducted on dots with sizes of 100 nm using LTEM, primarily because small magnetic volumes generate low contrast. Kirk *et al.*[7] carried out *in situ* TEM experiments on rectangular 300×80 nm^2-NiFe and Co dots (normally referred to as elements when noncircular), which were not found to be a single domain. Zweck *et al.*[8] studied the single domain 200-nm ellipses using Fresnel mode LTEM. The magnetization reversal *mechanism* could not be studied using this mode, and only the field at which the magnetization in the dots reversed was measured. The exact mechanism of moment rotation is still not understood. Single domain structures, which would be expected to reverse coherently, have been shown to deviate from this behavior,[9,10] presumably as a result of the presence of defects such as grain boundaries, crystallographic texture, edge defects, and irregularities in their shapes.

The magnetization reversal mechanisms of magnetic dots have also been investigated using micromagnetic modeling. These calculations involve solving time-dependent Landau-Lifshitz-Gilbert[11] (LLG) equations in order to determine the reversal mechanism. Various materials and configurations have been studied, and in some cases the results have shown good agreement with experimental results.[12–16] The general trend is, for models, to overestimate coercivity and saturation magnetizations as a result of the lack of consideration of microstructural defects, anisotropy, and other nonideal features. In the case of noncircular magnetic elements, the role of element ends as initiation points for magnetization reversal has been investigated.[17] Simulations have also been used to study the effect of magnetostatic interactions between dots in small arrays. Plateaux seen in hysteresis loops as a result of dot interactions have been predicted,[17,18] as has shearing of the hysteresis loop.[4] Moment rotation mechanisms such as end-initiated rotation,[19] the formation of vortex states and domain-wall nucleation and movement have all been observed in the simulations. In general, the smaller the dot and the closer its shape to an ellipse rather than a rectangle is, the closer the reversal mechanism is to single domain coherent rotation.

Here, we investigate quantitatively the internal magnetic structures of, and interactions between, square arrays of nominally identical 100-nm diameter and 20-nm-thick circular Co dots. The dots have an aspect ratio of 0.2, and in the absence of interactions they are expected to show in-plane magnetization and to be capable of supporting vortex configurations. We present images of magnetic remanent states in the dots obtained using both off-axis electron holography in the TEM and quantitative LTEM, from which interactions between the dots can be assessed. Some of the results presented here have been published in preliminary form elsewhere.[20]

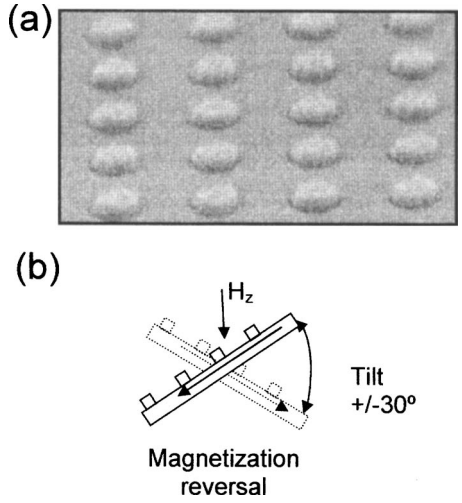

FIG. 1. (a) Scanning electron microscope image of nominally 100-nm diameter and 20-nm-thick Co dots fabricated on Si in a square array of side 200 nm. (b) Schematic diagram showing the experimental setup for applying an external magnetic field. H_z is the applied field direction, which is parallel to the electron microscope optic axis.

II. EXPERIMENTAL DETAILS

Large area arrays of Co dots were fabricated using interference lithography. In this process, a laser beam is split into two coherent waves, which are used to form an interference pattern on a substrate. Two interference patterns are used sequentially in order to expose a resist layer and to form a square array of holes. Magnetic dots are then fabricated using an evaporation and lift-off method. The details of the procedure are described in detail elsewhere.[21] Here, the substrate used was a silicon wafer, and the Co dots were nominally circular, 100 nm in diameter and 20 nm in thickness in a square array of period 200 nm, as seen in the scanning electron micrograph shown in Fig. 1(a). The dots were prepared for TEM examination in plan-view geometry by first thinning a piece of wafer from the substrate side to a thickness of ~ 50 μm using diamond paste. A 2×1-mm^2 piece of the thinned substrate with dots on it was cut and mounted, using conducting epoxy, onto a semicircular 3-mm-diameter Cu TEM ring. The sample was then milled using Ga ions in a focused ion-beam (FIB) system to form an electron-transparent window approximately 10×10 μm^2 in size and 100 nm in thickness, with the array of Co dots on one side.

Off-axis electron holography was carried out at 200 kV in a Philips CM200-ST TEM, equipped with an electron biprism. A detailed description of the technique of off-axis electron holography can be found elsewhere.[22] Holograms of magnetic remanent states were acquired by using a Lorentz mini lens which allows the specimen to be imaged in a magnetic-field-free environment with the conventional microscope objective lens switched off. The objective lens can, however, be switched on in order to apply a magnetic field to

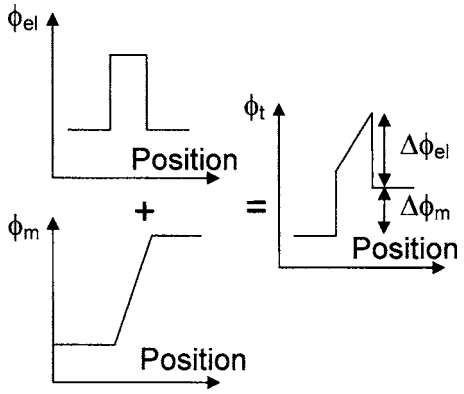

FIG. 2. Schematic diagrams showing the contributions to the phase shift of the electron wave that passes through a magnetic element. The top left diagram shows the electrostatic (mean inner potential) contribution ϕ_{el}, the bottom left diagram shows the magnetic contribution ϕ_m, and the diagram on the right shows the total phase shift ϕ_t.

the specimen. In order to record each magnetic remanent state, the sample was first tilted to +30° about the axis of the sample holder, and the objective lens was switched on in order to use the lens field to saturate the magnetization in the sample in one direction. The objective lens was then switched off, the sample tilted to −30°, and the objective lens current set to provide the desired component of magnetic field in the plane of the sample. Finally, the objective lens was switched off and the sample tilted back to 0° for acquiring holograms. It should be noted that the objective lens field is vertical, and thus a significant out-of-plane component of the applied field is present during the magnetizing process. The procedure was repeated for different values of applied field in order to build up a series of holograms around a remanent hysteresis loop. The field application approach is shown schematically in Fig. 1(b). Reference holograms were always recorded from vacuum in order to remove artifacts associated with the imaging and recording system of the microscope.

Following acquisition, the holograms were reconstructed to obtain the phase shift of the electron wave that had passed through the sample. The holograms contain both magnetic and electrostatic contributions to the phase shift, as shown schematically in Fig. 2. The electrostatic (mean inner potential) contribution to the phase shift results from the presence of variations in composition, density, and specimen thickness, while the gradient of the magnetic contribution to the phase shift is proportional to the in-plane component of the magnetic induction integrated in the electron-beam direction. For a nanoscale magnetic dot or element, the electrostatic contribution must be removed in order that the magnetic information of primary interest can be extracted.[23] Here, this separation was achieved by adding together the phase images that had been recorded around an entire remanent hysteresis loop. On the assumption that the magnetic contributions to the phase shift cancel out on average, the mean of the summed images contains only the electrostatic contribution to the phase shift. This average image can then be subtracted from each original phase image to leave only magnetic phase information. All image analysis and image processing were carried out using the SEMPER image processing package.[24] As errors and artefacts can result in nonperfect cancellation of the magnetic component in the summed images, this approach must be used with care. In the present experiments, the height of the step in the electrostatic contribution to the phase shift at the edge of each dot was of the order of 2 rad. This value is less than the 4.3 rad that would be predicted on the assumption that the dots have their nominal thickness and that the mean inner potential of Co is 22 V, suggesting that the dots are, in fact, less than 20 nm thick.

The same sample was investigated using the Fresnel mode of LTEM. The results were analyzed using the transport of intensity equation (TIE) in order to obtain quantitative phase information for comparison with the electron holography results.[25] Lorentz microscopy was carried out using a JEOL 4000EX TEM fitted with a Lorentz lens, which allows the sample to be imaged at 400 kV in a magnetic-field-free region, using a specialized sample holder that can be used to apply an in-plane magnetic field to the sample. Fresnel defocus images of the dots were recorded both at remanence and in applied in-plane fields of up to ±700 Oe. In each case, an image was recorded first in focus, and then a pair of images was recorded using defocus values of ±108 μm. The resolution of the TIE technique is determined in part by the defocus value during the experiment.[26,27] The defocus values were calibrated, with an error of less than 5%, by tilting a TEM grid with a fine mesh, refocusing and registering the change in the current of the objective lens. The combined magnetic and electrostatic phase contributions were extracted from these images by using the commercially available QPE software,[28] which provides a solution to TIE using a Fourier space approach.[29,30]

It should be noted that both electron holography and LTEM are only sensitive to the components of the three-dimensional magnetic vector field that are perpendicular to the direction of the electron beam. These components are in the plane of the dots when the sample is at zero tilt.

III. EXPERIMENTAL RESULTS AND DISCUSSION

Figure 3 shows the magnetic phase contours obtained directly from experimental electron holograms, with the sample in a different remanent state in each image. The white lines show the positions of the Co dots. In the on-line version of this paper, the images have been color coded, with both colors and arrows indicating the local direction of the measured magnetic induction. The contours in each image are lines of equal phase. The spacing between them (0.0625 rad) is inversely proportional to the in-plane component of the magnetic induction integrated in the electron-beam direction. The phase images in Fig. 3 show a large variation in magnetization direction between different dots within the array, as well as the demagnetizing fields between the dots. Many of the dots are single domain, with parallel contours. However, some dots have a 90° change in the direction of the contours within them [for example, dot 8 in (b), the number is referring to the inset in Fig. 4, note however, dots 1–4 are not shown in Fig. 3]. Several dots appear to show the presence of vortices [for example, dot 10 in Fig. 3(h)], which are associated with complete rotation of the contours into a closed

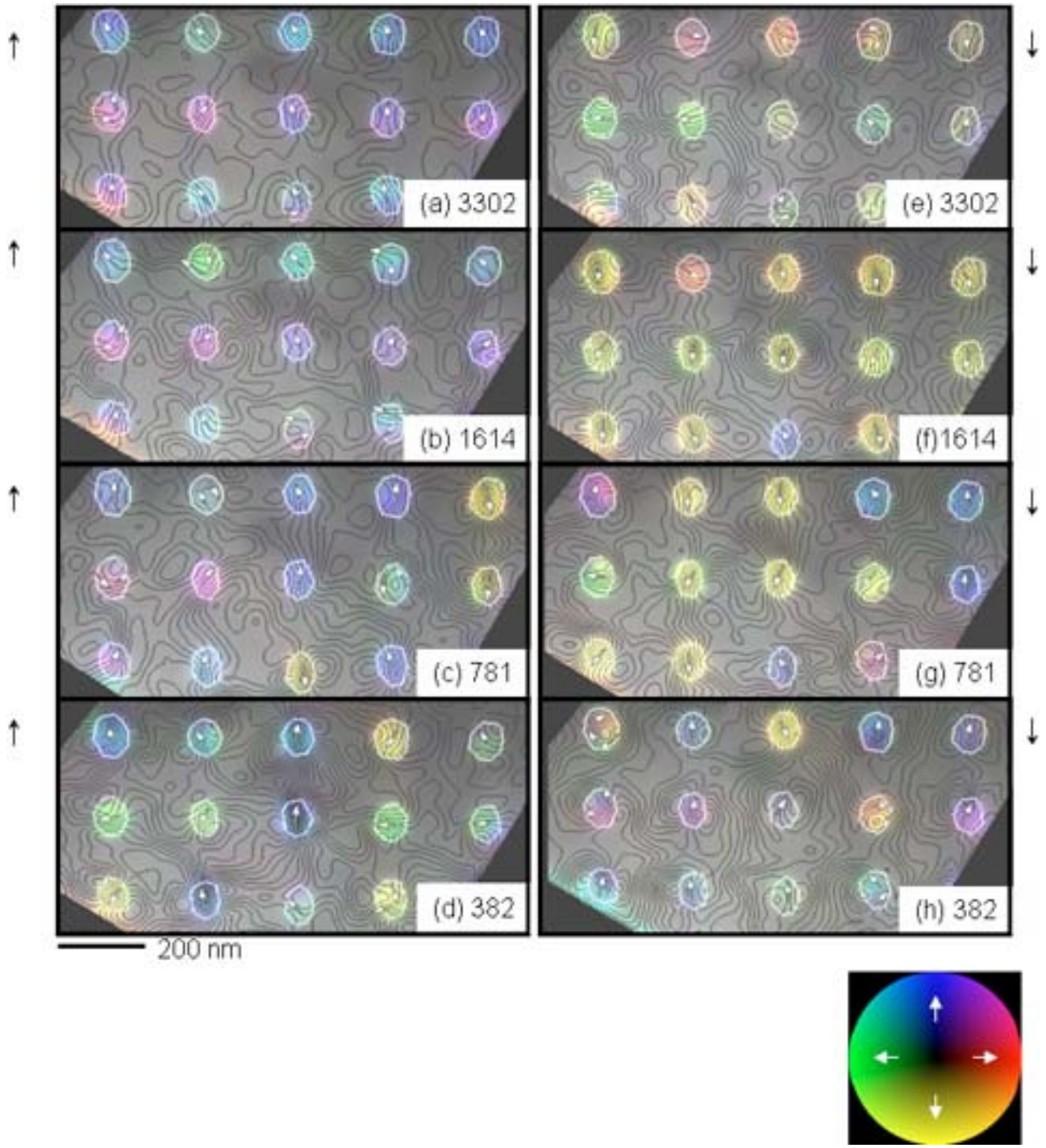

FIG. 3. (Color online) Magnetic induction maps showing remanent states in the square array of Co dots measured using electron holography. The spacing between adjacent contours is 0.0625 rad. The applied fields in oersted are shown, with ↑ and ↓ indicating the directions of the indicated applied in-plane field after saturation in the opposite direction. The color wheel indicates the direction of magnetization by the color and the intensity represents the strength of the magnetic signal.

loop. These vortices are generally displaced towards the edges of the dots, suggesting that they may not be large enough to support centred vortex configurations. Many of the dots appear to be coupled to each other magnetically in rows [see, for example, Fig. 3(a)], with alternating rows having their magnetization directions rotated with respect to each other by angles of up to ±30°, forming "zigzag" or "herringbone" patterns. This observation indicates that there is relatively strong coupling between adjacent rows of dots, which are orientated perpendicular to the applied field direction. This coupling is not seen if the deviation angle is plotted by column rather than by row. This difference may result from the fact that the dots are slightly elongated in the direction of the applied field.

The angles of the magnetic phase contours in the dots are quantified in Fig. 4, for an image acquired at an applied field of −47 Oe (not shown in Fig. 3). The position of the end of each row is shown using a black line in the graph, and the

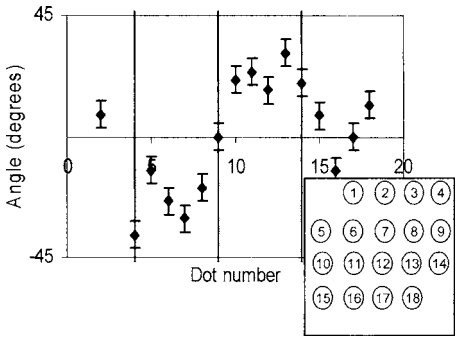

FIG. 4. Angles of the measured magnetic phase contours from the applied field direction for an in-plane field of 47 Oe. A positive angle represents a clockwise rotation. The black lines indicate the ends of the rows of dots. The dot positions are indicated in the inset.

schematic positions of the dots are shown as an inset. A clear, regularly varying pattern of angles is seen with row number. Analysis of other images in the series shows that as the applied reverse field increases so the angle of deviation away from the applied field direction in the remanent states also increases, until the magnetization direction reverses. This observation suggests that magnetization reversal in nanodot arrays is associated with interdot coupling, which may in turn be facilitated by pinning of the magnetization by defects, such as grain boundaries and edge irregularities. These effects may partially explain the increase in coercivity observed in such arrays of dots from the theoretical in-plane value of zero.

A remanent hysteresis loop, derived from the experimental phase images in Fig. 3, is shown in Fig. 5. A corresponding hysteresis loop obtained from approximately 6×10^{10} dots using vibrating sample magnetometry (VSM) is shown in Fig. 6. The remanent hysteresis loop shown in Fig. 5 was calculated by counting the number of dots magnetized primarily parallel and antiparallel to the applied field direction, normalizing this value by dividing by the number of dots, and plotting the result as a function of the applied in-plane field. For dots in which the contours were perpendicular to the applied field direction, a magnetic induction of zero was assigned. If the contours were at an angle to the applied field, then the value was rounded either to the applied field direction if the angle of deviation was less than 45° or to zero if the angle was greater than 45°. Each point in Fig. 5 is an average of measurements from 18 dots. A mean coercivity of 380 (±20) Oe was calculated from this hysteresis loop, as compared with a value of 220 Oe reported previously from

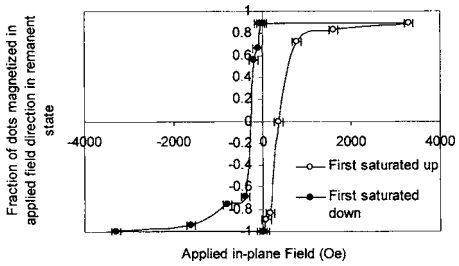

FIG. 5. Remanent hysteresis loop plotted by counting the number of dots pointing either up or down, and dividing by the number of dots considered.

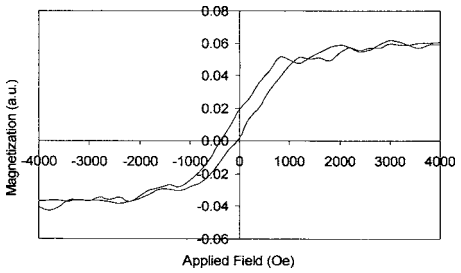

FIG. 6. In-plane hysteresis loop for $\sim6\times10^{10}$ dots measured using VSM.

the VSM hysteresis loop shown in Fig. 6.[21] Both the loop obtained using VSM and the remanent loop obtained from the electron holographic phase images show appreciable variability in the switching fields of the nominally identical dots. This variability is thought to arise from the effects of magnetostatic interactions between adjacent dots and from microstructural differences between them.

The variation in the in-plane component of the magnetic induction between different dots in the array was measured as a function of applied field by counting the number of contours (i.e., the phase change) across each dot in a direction perpendicular to the applied field direction. The results of these measurements are shown in Fig. 7. It should be noted that the sample was saturated magnetically between successive images, which therefore do not constitute parts of the same magnetization reversal process. The observed variability cannot result from the damage induced during the TEM sample preparation process, as measurements from individual dots vary with applied field. On the assumption that the differences are not caused by demagnetizing fields, the most likely explanation is that differences in microstructure, grain size, grain orientation, defect density, and degree of oxidation, together with interdot coupling, can result in the partial out-of-plane magnetization of each dot, which occurs to a different extent for each value of the applied field. For values of the applied field at which the dots are aligned magnetically (for example, see Fig. 3(f)), the number of contours in each dot is very similar; presumably as a result of either strong in-plane coupling or a lack of strong out-of-plane coupling between the dots.

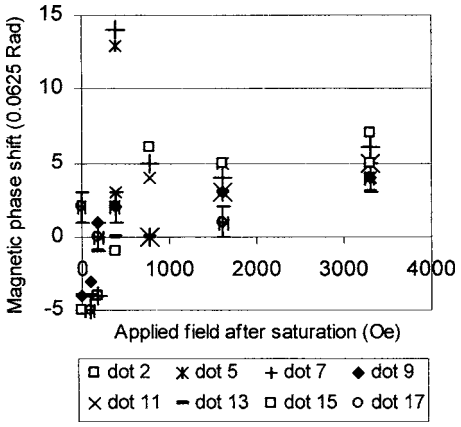

FIG. 7. In-plane magnetic phase shifts across individual dots, measured in a direction perpendicular to the applied field. Dot numbers refer to Fig. 4 inset.

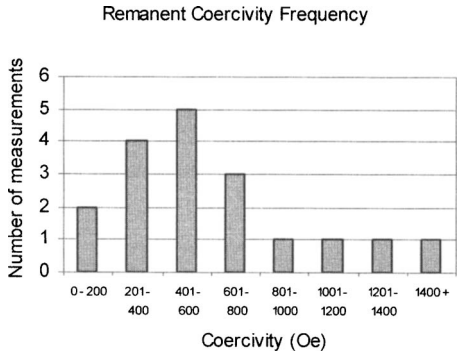

FIG. 8. Frequency plot of the coercivity values of individual dots. The mean value of the coercivity is 670±403 Oe. The large standard deviation results from the spread in the magnetic properties of the dots, and not from the experimental error.

Neither electron holography nor LTEM is sensitive to the presence of an out-of-plane component of the magnetic induction. The out-of-plane hard axis coercivity of the sample is 100 Oe (measured by VSM), and the remanence is small but nonzero, suggesting that a component of magnetization normal to the plane of the dots is then present. When the objective lens field is applied to the dots, both an in-plane and an out-of-plane components of the applied field are present. The out-of-plane component is larger than the in-plane component by a factor of $\sqrt{3}$. For example, for an in-plane applied field of 3300 Oe, the field perpendicular to the plane of the sample is 5700 Oe. When the sample is imaged at remanence, any out-of-plane component of the magnetization is expected to relax substantially. The demagnetizing factor N is the constant of proportionality in the relation $H=NM$ between the magnetization (M) and the applied magnetic field (H), and depends solely on the geometry of the sample. For the dots analyzed here, the demagnetizing factor can be calculated from the expressions:

$$\frac{N_a}{4\pi}=\frac{N_b}{4\pi}=\frac{\pi}{4m}-\frac{1}{m^2} \quad \text{and} \quad \frac{N_c}{4\pi}=1-\frac{\pi}{2m}+\frac{2}{m^2}, \qquad (1)$$

where N is the demagnetizing factor along a, b, or c, $a=b$ is the diameter of the dot, and c is its measured thickness of ~10 nm, with $m=a/c$.[31] For the present sample, $N_a/4\pi=0.079$ and $N_c/4\pi=0.863$, indicating a strong preference for in-plane magnetization. (The demagnetizing factor is not the same as the reduction in the number of electron holographic contours that result from the stray field of a single dot.) The most likely explanation for the unexpected variation in the measured induction in each individual dot is that different images correspond to the formation of different magnetic states, for the reasons mentioned above. This is a very interesting point, suggesting that magnetic configurations in individual circular dots may not be consistently repeatable in the manner that is expected to be required for information storage applications.

The large variation in the measured coercivity between individual dots, which is shown in Fig. 8, could result from several factors. Sample preparation for electron microscopy may have resulted in greater amounts of Ga implantation or damage to some dots, with the Ga-contaminated dots being magnetically harder than others.[32] In addition, structural variations, such as edge roughness and randomly varying magnetocrystalline anisotropy in the polycrystalline dots, will make some dots magnetically harder than others. Finally, magnetostatic interactions between the dots affect the external field required to achieve reversal. The overall energy of the system is clearly reduced if flux closure occurs between groups of dots.[33] This effect is an important consideration for data storage applications, firstly because the applied field needed to reverse the magnetization direction of each dot should ideally be independent of the magnetization state of its neighbors, and secondly because the reversal field of each dot needs to be the same within a narrow applied field range. If the reversal field of a particular dot is increased by the formation of a flux closure state with its neighbors, then this behavior is detrimental to their use as a data storage medium. This effect could be minimized by increasing the interdot spacing or by changing the shape or the aspect ratio of the dots, and further work is required to determine the effect of these parameters on the degree of interaction.

Several of the dots show magnetic vortex states at remanence for intermediate values of the applied field. This observation can be compared with the previous work, in which the magnetization reversal of circular permalloy disks of diameter 350 nm was shown to proceed by the creation, propagation, and annihilation of magnetic vortices.[34] In addition, several dots appear to be able to support 90° domain walls. This is in good agreement with work by Scholz *et al.* who predict that for the dimensions of the dots in question the magnetic state is on the boundary of in-plane single domain and vortex or multidomain behavior.[35] The presence of all of these features suggests that complex reversal mechanisms may be taking place. For example, magnetization reversal may involve the formation of either a 90° wall or a vortex, which may then uncurl to complete the reversal process.

LTEM was also used to study the dots, by using an experimental setup in which the external field is applied in the plane of the sample by using magnetizing coils in the TEM specimen holder, rather than by tilting the sample and using the objective lens field. The effect of the significant out-of-plane applied field, which was present in the holography experiments, can be eliminated in this way. Figure 9(a) shows the Fresnel mode defocus images of the dots, while Fig. 9(b) shows the result of quantitative phase reconstruction using the TIE approach for an applied field of 700 Oe. The Fresnel images in Fig. 9(a) shows the presence of domain walls (dark or light lines) and magnetic vortices (light or dark spots) in some of the dots. The magnetic contribution to the phase shift can be measured from a line profile across a dot in the phase image, as shown in Fig. 9(c). The line profiles have been corrected for contrast gradients in the phase image, which arise from boundary effects and noise on the solution of the TIE. This correction involved taking a line profile on each side of the dot, calculating the average gradient of these profiles and subtracting this background to adjust the phase ramp. A line profile was also taken parallel to the applied field direction, as shown in Fig. 9(c). This profile should contain no magnetic phase change if the dot is magnetized parallel to the applied field direction. An average value of

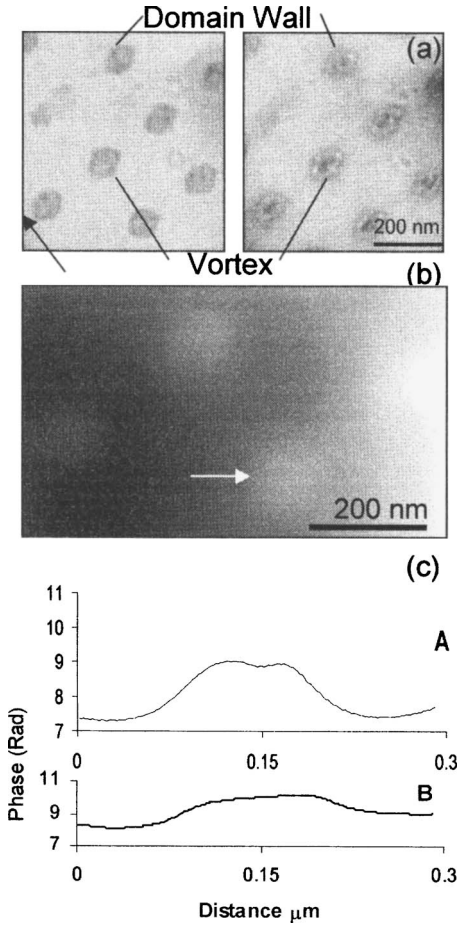

FIG. 9. (a) Fresnel defocus images acquired at ±108-μm defocus. The arrow indicates the applied field direction. (b) Phase image [bottom 4 dots from (a)] obtained by applying the transport of intensity equation to the Fresnel TEM images. (c) Corresponding line profiles indicating the phase changes across the dot indicated with the white arrow in (b), both parallel (A) and perpendicular (B) to the applied field direction.

0.01 (±0.005) rad/nm for the phase gradient across a dot was measured from 16 dots. This value is higher than the average gradient of 0.0043 rad/nm measured from 18 dots using electron holography, indicating that the mechanism of applying the field in the holography experiment may have introduced some out-of-plane contribution to the magnetization. An important point to note is that both of these values are considerably lower than the value of 0.046 rad/nm that would be predicted for the expected phase change in individual isolated dots calculated using Eq. (2),

$$\Delta\varphi = \left(\frac{e}{\hbar}\right) B_{\perp} t d, \tag{2}$$

where $\Delta\varphi$ is the phase change due to the magnetic induction, $B_{\perp}$ is the induction perpendicular to the electron-beam direction, t is the nominal dot thickness, and d is the dot diameter. This discrepancy may be accounted for by a combination of several factors. Firstly, it was shown above that the true thickness of the dots is approximately half of the nominal value. Secondly the dots are slightly conical, with a top diameter of 80 nm and a base diameter of 100 nm, and also slightly elliptical with a minor axis of ~80 nm and a major axis of 100 nm. This reduction in the volume of magnetic material reduces the expected phase change by a factor of 0.8. Thirdly, there is oxidation of the dots, which was investigated by the analysis of the L_3 and L_2 Co edges, and by the presence of a strong oxygen K edge in electron-energy-loss spectra.[36,37] For an array of dots there is a reduction in the expected magnetic phase shift across a dot due to the demagnetizing fields of neighboring dots. In the case of these dots in a square array, this reduces the expected phase shift to 0.038 rad/nm. Furthermore, relaxation of the magnetization from the saturation configuration will occur when the applied field is removed. It should be noted that the electrostatic potential contribution to the phase shift measured using TIE was of the order of 1.5 rad between the silicon substrate and the Co dot, which is similar to the value obtained using electron holography. This measurement is shown in the line plot labeled A in Fig. 9(c).

IV. CONCLUSIONS

We have used off-axis electron holography to record the magnetic induction maps of remanent states from an array of nominally identical 100-nm diameter and 20-nm-thick Co dots. A large proportion of the dots are single domain, with a magnetization direction that deviates only slightly from the applied field direction. This deviation may be associated with magnetostatic interactions between adjacent rows of dots. For small values of the applied field, the remanent states can also include magnetic vortices and domain walls. The magnetization reversal process may therefore proceed by a mechanism involving these states, rather than by the uniform rotation of the magnetic moments. The magnetic induction measured from the magnetic contribution to the electron holographic phase shift is approximately 1/10 of that predicted for bulk Co. This discrepancy may be explained by a combination of a slightly smaller dots size than the nominal value, oxidation of the dots, demagnetizing fields, and an out-of-plane component of their magnetization, which cannot be detected using electron microscopy for samples in this geometry. We have also obtained quantitative phase information from the same dots using Lorentz microscopy and the transport of intensity equation. The values of the magnetic phase gradient across the dots are twice those measured using electron holography, most likely as a result of the use of a solely in-plane applied magnetic field in the Lorentz experiment.

ACKNOWLEDGMENTS

We thank R. C. Doole for help with Lorentz microscopy, D. Kirk for help with EELS and Professor M. R. McCartney for help with the electron holography, and Professor G. W. Smith and Professor D. J. Fray for the provision of laboratory space. One of the authors (T.J.B.) acknowledges funding from the EPSRC. Another author (C.A.R.) acknowledges the NSF for financial support and M. Farhoud for sample fabrication. Another author (R.E.D.) is grateful to the Royal Society for financial support. We acknowledge the use of facilities at the John M. Cowley Center for High-Resolution Electron Microscopy at Arizona State University, USA.

[1]S. Y. Chou, Proc. IEEE **85**, 652 (1997).
[2]S. Y. Chou, P. R. Krauss, and L. Kong, J. Appl. Phys. **79**, 6101 (1996).
[3]F. Rousseaux *et al.*, J. Vac. Sci. Technol. B **17**, 3168 (1999).
[4]C. A. Ross, M. Farhoud, M. Hwang, H. I. Smith, M. Redjdal, and F. B. Humphrey, J. Appl. Phys. **89**, 1310 (2001).
[5]K. Yu, S. Choe, and S. Shin, Appl. Phys. Lett. **76**, 3609 (2000).
[6]F. Porrati and M. Huth, Appl. Phys. Lett. **85**, 3157 (2004).
[7]K. J. Kirk, J. N. Chapman, S. McVitie, P. R. Aitchison, and C. D. W. Wilkinson, J. Appl. Phys. **87**, 5105 (2000).
[8]J. Zweck, S. Bräundl, S. Henzelmann, M. Schneider, S. Otto, M. Heumann, and T. Uhlig, Scr. Mater. **48**, 967 (2003).
[9]D. D. Awschalom and D. P. di Vencenzo, Phys. Today **48**(4), 43 (1995).
[10]M. Lederman, S. Schultz, and M. Ozaki, Phys. Rev. Lett. **73**, 1986 (1994).
[11]L. Landau and E. F. Lifshitz, Phys. Z. Sowjetunion **8**, 153 (1935).
[12]C. A. Ross *et al.*, Phys. Rev. B **62**, 14252 (2000).
[13]T. Schrefl, J. Fidler, K. J. Kirk, and J. N. Chapman, J. Appl. Phys. **85**, 6169 (1999).
[14]D. R. Fredkin and T. R. Koehler, J. Appl. Phys. **67**, 5544 (1990).
[15]M. Schneider, H. Hoffmann, and J. Zweck, J. Magn. Magn. Mater. **257**, 1 (2003).
[16]R. E. Dunin-Borkowski, M. R. McCartney, B. Kardynal, D. J. Smith, and M. R. Scheinfein, Appl. Phys. Lett. **75**, 2641 (1999).
[17]P. H. W. Ridley, G. W. Roberts, R. W. Chantrell, K. J. Kirk, and J. N. Chapman, IEEE Trans. Magn. **36**, 3161 (2000).
[18]W. Chen, D. R. Fredkin, and T. R. Koehler, IEEE Trans. Magn. **28**, 3168 (1992).
[19]Y. D. Yan and E. D. Torre, J. Appl. Phys. **66**, 320 (1989).
[20]R. E. Dunin-Borkowski, S. B. Newcomb, M. R. McCartney, C. A. Ross, and M. Farhoud, Inst. Phys. Conf. Ser. **168**, 485 (2001).
[21]M. Farhoud, J. Ferrera, T. J. Lochtefeld, T. E. Murphy, M. L. Schattenburg, J. M. Carter, C. A. Ross, and H. I. Smith, J. Vac. Sci. Technol. B **17**, 3182 (1999).
[22]R. E. Dunin-Borkowski, M. R. McCartney, and D. J. Smith, in *Encyclopedia of Nanoscience and Nanotechnology*, edited by H. S. Nalwa (American Scientific, California, 2004), Vol. 3, pp. 41–100.
[23]R. E. Dunin-Borkowski, M. R. McCartney, D. J. Smith, and S. S. P. Parkin, Ultramicroscopy **74**, 61 (1998).
[24]W. O. Saxton, T. J. Pitt, and M. Horner, Ultramicroscopy **4**, 343 (1979).
[25]*Magnetic Imaging and its Applications to Materials*, edited by M. de Graef (Academic, San Diego, CA, 2001).
[26]P. Donnadieu, M. Verdier, G. Berthom, and P. Mur, Ultramicroscopy **100**, 79 (2004).
[27]M. Beleggia, M. A. Schofield, V. V. Volkov, and Y. Zhu, Ultramicroscopy **100**, 37 (2004).
[28]http://www.iatia.com.au/
[29]D. Paganin and K. A. Nugent, Phys. Rev. Lett. **80**, 2586 (1998).
[30]V. V. Volkov and Y. Zhu, Phys. Rev. Lett. **91**, 043904 (2003).
[31]J. A. Osborn, Phys. Rev. **67**, 351 (1945).
[32]D. Ozkaya, R. M. Langford, W. L. Chan, and A. K. Petford-Long, J. Appl. Phys. **91**, 9937 (2002).
[33]R. J. Harrison, R. E. Dunin-Borkowski, and A. Putnis, Proc. Natl. Acad. Sci. U.S.A. **99**, 16556 (2002).
[34]M. Schneider, H. Hoffmann, and J. Zweck, J. Magn. Magn. Mater. **257**, 1 (2003).
[35]W. Scholz, K. Yu. Guslienko, V. Novosad, D. Suess, T. Schrefl, R. W. Chantrell, and J. Fidler, J. Magn. Magn. Mater. **266**, 155 (2003).
[36]Z. L. Wang, J. S. Yin, and Y. D. Jiang, Micron **31**, 571 (2000).
[37]D. H. Pearson, C. C. Ahn, and B. Fultz, Phys. Rev. B **47**, 8471 (1993).